International Scholarly Research Network
ISRN Spectroscopy
Volume 2012, Article ID 868561, 8 pages
doi:10.5402/2012/868561

Research Article

Experimental Study of Laser-Induced Brass and Copper Plasma for Spectroscopic Applications

Ardian B. Gojani

Institute of Fluid Science, Tohoku University, 2-1-1 Katahira, Aoba, Sendai 980-8577, Japan

Correspondence should be addressed to Ardian B. Gojani, gojani@edge.ifs.tohoku.ac.jp

Received 16 March 2012; Accepted 23 April 2012

Academic Editors: S. Harilal, U. Pal, and M. Soylak

This paper presents time-resolved and space-integrated laser-induced breakdown spectroscopic (LIBS) analysis of copper and brass plasma. It was observed that copper emission is very strong during the first hundred nanoseconds of the plasma, but then some lines (e.g., at 327.4 nm) decrease in intensity, while others (e.g., 521.8 nm) slightly increase. Zinc lines, on the other hand, did not decrease significantly in intensity even two microseconds after ablation, but they became narrower due to the decrease of the density of free electrons. Copper line intensities showed the same characteristics regardless whether the plasma was created in a metallic copper or brass sample. Assuming local thermodynamic equilibrium, plasma temperature, and electron density is obtained from Boltzmann plot and Lorentzian profile fitting, respectively. The effect of subsequent irradiation on the same spot was investigated, and the number of necessary shots for surface cleaning was determined.

1. Introduction

Laser-induced breakdown spectroscopy (LIBS) has reached an advanced level of development as a technique for elemental analysis and plasma diagnostics, with several published books and review papers covering many aspects of its nature and applications [1–6]. The great potential of LIBS lays in the simplicity of its setup: a pulsed laser beam with sufficient energy (usually several tens of mJ) is focused onto a target surface so that to cause its ablation, leading to rapid generation of an expanding plasma. Plasma contains excited atoms, ions, and molecules that emit light with characteristic wavelengths upon relaxation. Collection and analysis of the plasma light reveals the constituent elements of the interrogated surface, as well as their state (ionization level, temperature, and electron density).

Despite numerous studies on LIBS, there remain quite a few challenges for the development of a turn-key LIBS system, which require some laboratory work. In particular, LIBS signal depends critically on the properties of the plasma, such as temperature and electron density, and these, in turn, vary significantly on a great range of values of laser parameters (beam energy, duration, wavelength, focusing), physical and chemical properties of the sample (composition, material matrix), the ambient in which the plasma is expanding (gas composition, state of flow, pressure), the signal acquisition systems (ICCD versus CCD cameras, acquisition time delay and acquisition time window), just to name a few. Hence, a full description of LIBS signal requires a full command or knowledge of the experimental (external) parameters.

Among several recent investigations on LIBS, a considerable attention is given to the development of a calibration-free and robust LIBS system that can find applications for geological explorations of lunar and planetary environments, with two recent examples of LIBS being applied for these purposes to be found in the papers by Rauschenbach et al. [7] and Lanza et al. [8]. The aim is to develop a system that can minimize external effects, while yielding fast, accurate, and repeatable data, as well as improving analytic detection. Since plasma plays the most important role in the LIBS signal, we have experimentally studied the characteristics of plasma created by ablation of copper and brass coupons by using an LIBS system. There are many experimental and theoretical studies reported in the literature that cover the effects of the above-mentioned factors on LIBS performance. The role of ablation on spectrochemical analysis is discussed by Russo et al. [9]. Fornarini et al. [10] have studied the influence of laser wavelength (355 nm and 1064 nm) upon the analytical

results obtained from applying LIBS diagnostics to bronze. Shaikh et al. [11] and Qindeel et al. [12] studied the effect of three different wavelengths from Nd : YAG laser (355 nm, 532 nm, and 1064 nm) on zinc and cadmium plasmas that propagated in four different atmospheres: air, helium, argon, and neon, by measuring the evolution of electron number density and temperature. Cristoforetti et al. [13] studied the role of the ambient pressure on the LIBS of brass samples, also by looking at the single and double pulse configurations. The effect of laser pulse duration on plasma signature was reported by Rieger et al. [14] and Le Drogoff et al. [15]. Instrumentation also plays a major role in LIBS signals, as evidenced by the study of Unnikrishnan et al. [16]. Brass has also been studied extensively, either using inductively coupled or laser-induced plasmas [17–22], with the main interest being that as a binary alloy characterized by a large difference in thermal properties of copper and zinc, brass presents a good example to study preferential ablation.

This paper presents an experimental study on plasma spectroscopy of copper and brass samples with the aim at utilizing plasma for material characterization. Our previous work on ablation of metals [23] did not show a considerable difference in mass ablation of zinc, copper, and brass under similar conditions as presented in this paper. Now we experimentally study the line emission kinetics and determine electron number densities and temperatures for plasma obtained by the contribution of copper and zinc emissions of brass sample. Also, we look at the behavior of copper plasma from both pure copper and brass samples, in order to see if there is any difference (as expected) due to matrix effects. This work follows on the application of calibration-free LIBS in geology, for example, for elemental analysis of rocky samples. Hence, we started with simple samples that are composed mainly of one (pure copper) and two metallic elements (brass). The only external factor investigated is the role of the system for collection of plasma radiation, which is achieved from two different positions, albeit in space-integrated mode. Other factors, such as laser energy, pulse, wavelength, and focusing spot, are kept constant.

2. Experiment

Plasma for LIBS analysis was generated by focusing a laser beam using a 100 mm focal length lens into a 100 μm diameter spot on the surface of the target. Laser beam has the following parameters: energy 25 mJ, wavelength 532 nm, and pulse duration 3 ns. For an optical system with M2 factor approximately 1.5, the calculated fluence then is about 100 J/cm^2 (irradiance ~30 GW/cm^2). These values are above the threshold for solid breakdown, but still considerably below the threshold values for laboratory air breakdown. This irradiance is also high enough to ablate a considerable target mass, yielding negligible fractionation effects.

Two types of targets were used: 1 mm thick coupons of copper (~99% Cu) and brass (~60% Cu, ~40% Zn), with dimensions 40 mm × 40 mm. One set of data was collected from the plasma generated by the ablation of a fresh target surface, and a second set of data was collected by repeatedly ablating a fixed spot.

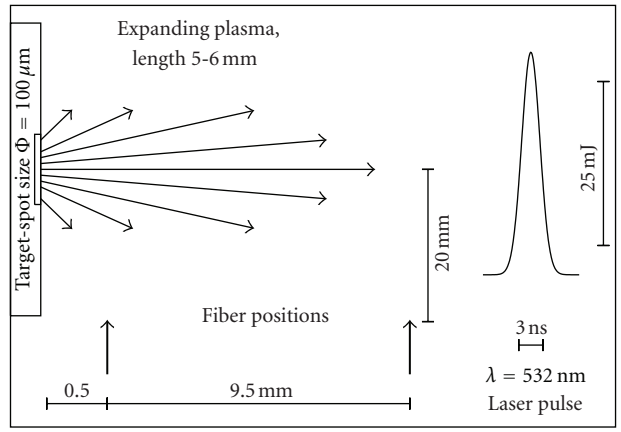

Figure 1: Top view of the placement of the collecting fiber shown by thick arrows (not to scale).

Laser-induced plasma light was collected by an optical fiber with a 50 μm diameter core. The fiber was placed at two different positions, as shown in Figure 1, which gives the top view perspective. In the sketch, the laser beam is incident from the right, that is, opposite to the direction of the plasma expansion which is depicted by the expanding thin arrows. The thick left arrow on the bottom shows the placement of the fiber core 0.5 mm from the surface of the target, and the one in the right shows the position of the fiber core 10 mm from the target surface. In both cases, the fiber core height from the optical bench is the same as the central position of the plasma. The front face of the fiber is placed 20 mm from the central line of the plasma. Since the fiber has a viewing angle of 28 degrees, from this distance it will see the length of about 10 mm at the central line of plasma. This length is longer than the plasma itself, which, considering the luminous volume, is estimated to be about 5-6 mm. Hence, all the spectra shown in the following are space integrated.

Plasma light is cross-dispersed by an echelle grating spectrograph in the wavelength range from 200 to 900 nm. The minimal resolving power of the spectrograph ($\lambda/\Delta\lambda$) along this entire range is 5000, with wavelength resolution of 0.01 nm in the ultraviolet and 0.05 nm in the visible range. Nine lines from a mercury lamp are used for wavelength calibrations, and lines at 296.73 nm and 576.96 nm are used to obtain the instrument function (apparatus profile). The respective FWHM values of the instrument function at these wavelengths are 0.07 nm and 0.11 nm.

The dispersed light is recorded by a gated ICCD camera with varying quantum efficiency along the wavelength range. The camera is operated in the intensified mode for 100 ns, and this value defines the time resolution of the measurement. A digital delay generator combined with a fast photodetector and a high-speed oscilloscope is used to synchronize the laser and the spectrometer, achieving four distinct times of measurement: 0.34 μs, 0.64 μs, 1.28 μs, and 2.28 μs after the laser pulse. The choice of the earliest moment for time-resolved measurement is decided on 0.34 μs because at earlier times plasma is not well suited (it might be in a state of radiation disequilibrium), and many processes have not reached

their stable conditions; for example, externally propagating shock waves have not been established, or internally propagating shock waves would be present, thus precluding stability of the plasma. At the other end, the latest moment for time-resolved measurements was decided on 2.28 μs into the life of plasma because at later times LIBS is usually conducted in time-integrating mode due to the decrease of the line intensities.

Correspondence of an emission line to a particular chemical element, as well as the data for each line, such as transition probabilities, statistical weights, and energies of the levels, is consulted from the NIST database [24].

3. Results and Discussion

3.1. Identification of Elements. Identification of the wavelengths of the emission lines from different atoms, ions, and/or molecules lies at the core of applications of LIBS for elemental analysis, and usually this is done in a semi-automatic fashion by comparing the most intense plasma line emissions to a database of such lines. Application of a peak detection algorithm based on local maximum identified more than 80 peaks per spectra, which had to be manually verified. Out of these, about 30 lines that showed consistency were further analyzed and compared to the NIST database. An example is shown in Figure 2, where the single-shot spectra from a copper and a brass sample are given, with the noted copper and zinc lines. In applications of LIBS for elemental analysis, the spectral resolution of the spectrometer is crucial. Echelle grating spectrometers are sophisticated instruments with very good resolutions, which help in identifying different elements that have close emission lines, for example, the neutral emission lines of zinc at 330.2 nm and copper at 330.7 nm. However, resolving two lines does not depend only on the dispersive instrument, but on the properties of the plasma, as well. Although the two mentioned lines have a wavelength difference that even moderate spectrometers can resolve, in the initial moments of the life of plasma these lines are very wide and overlap. This is due to high electron density and the large number of collisions which lead to continuum bremsstrahlung radiation. This also hampers the fully automatic distinction of lines, as illustrated in Figure 3, where the spectra from brass for different times are given. Inspecting the two lines (330.2 nm and 330.7 nm) in the spectrum obtained at 0.32 μs, one finds that they do not pass the Rayleigh criterion for being considered as resolved lines [25]. In later stages of the life of plasma (even at 0.64 μs for fiber placed 0.5 mm from the surface of the target and at 1.28 μs for the fiber placed 10 mm from the surface), with the decrease of the continuum radiation, these lines become clearly distinguishable. In the same graph, the intense molecular nitrogen emission at 337.1 nm is not present even at later times, testifying to the lack of air breakdown. In fact, in all these experiments the emissions from air constituents that would otherwise be present in the case of air breakdown [26], for example, lines O II at 407.6 nm and N II at 399.5 nm at initial times, and O I and N I multiplets at 394 nm and 414 nm at later times, were absent. This not only confirms that laser ablation and plasma expansion

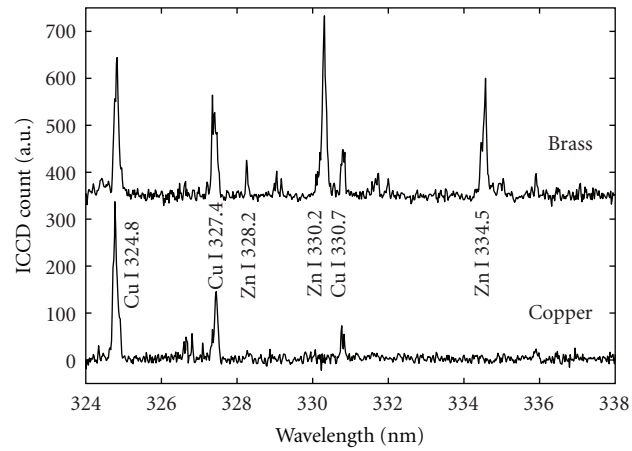

Figure 2: Single-shot spectra from a copper and a brass sample (shifted for clarity, with the intensity preserved).

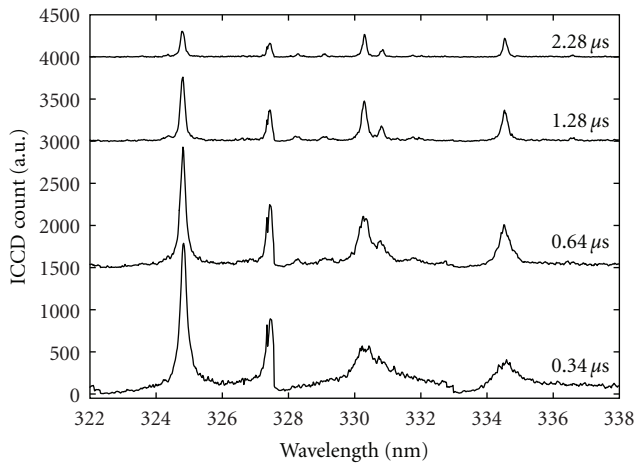

Figure 3: Time-resolved spectra for brass (shifted for clarity, with the intensity preserved).

did not cause air breakdown but also helps in identifying certain lines. An example is the case for the line at 404.3 nm, which could have been an emission from singly ionized nitrogen, but, based on the above, this line corresponds to emission from singly ionized copper. Neutral copper has two close lines at 324.3 nm and 324.7 nm with respective relative intensity ratios ~1/6. In our well-resolved spectra, the former line appears only after the continuum radiation has decreased significantly, which for this case happens after 1.28 μs into the life of plasma.

3.2. The Effect of Successive Ablation. It is a common practice when doing LIBS that one ablates the sample surface with several pulses before collecting spectra, the aim being cleaning the surface from elemental impurities on the surface, such as oxides or other adsorbed metallic atoms. In the present experiments, the effect of the number of pulses on the LIBS signal was tested by successively ablating the same spot and collecting the signal after each individual ablation. In this case, successive laser pulses were irradiated with 3-4 seconds

delay, which is long enough for the ablation plume to expand and condense on the surface and sufficient to minimize the possible plasma reheating effects. Hence, all the presented LIBS experiments are of a single pulse type, rather than dual or multiple pulse LIBS.

Comparison of spectra obtained by ablating a fresh surface and a surface that has been ablated several times (up to ten) did show some minor differences, as shown in Figure 4, for a few neutral copper and zinc lines and for singly ionized zinc atom emitting at 255.8 nm. In this figure, normalized intensity represents the ratio of the intensity of the line after the ablation pulse to the maximum intensity in the series for that particular line. Specifically, the plasma from the ablation of the fresh surface shows strong lines at 393.4 nm and 396.9 nm, which decrease in intensity on the second and third pulse and completely vanish on the fourth pulse and onwards, having absolute intensities comparable to the background levels (the maximal value of the background is presented in the figure by the horizontal dashed line). These emission lines always showed as a pair, with the second one more intense. Also, they appeared only on the brass samples, but not on the copper samples thus dismissing the possibility of the line 393.4 nm belonging to the singly ionized copper. Based on this, the emission of these lines can be attributed to traces of pollutant elements on the surface of the sample, most probably calcium. Similar behavior was observed for lines at 279.4 nm, 280.4 nm, and 657.1 nm, which are assumed to belong to traces of manganese and iron on the surface of the samples. Characteristic lines of copper and zinc increased in intensity after the first ablation pulse. Constancy of the intensity of the lines after the second or third successive pulse reveals that the dominant ablation mechanism is phase explosion, and a homogeneous mass of the material is removed with each pulse. Otherwise, if laser heating and evaporation would dominate the ablation process, zinc lines would become weaker and copper lines stronger, because zinc has a lower temperature of vaporization, and each successive pulse would leave a crater richer on copper. Similar behavior to the one shown in Figure 4 is observed even at later times, with the difference that some lines, for example, Zn II at 255.8 nm, were absent. Some other lines, such as those at 361 nm, 441.5 nm, 469.8 nm, 543 nm, to name a few, were identified as emissions from neutral iron atoms and were present from both brass and copper samples. Since these lines did not decrease in intensity with the increase of the number of pulses, we conclude that iron is present in the bulk of the samples and not only on the surface. Due to their large widths and very low intensities (signal-to-noise ratio ~3), these iron lines were not considered for characterizing the plasma. In the case of emissions characteristic of copper, the lines showed the same behavior regardless whether the sample was brass or copper.

3.3. Light Collecting Fiber Placement. The position of the fiber that collects the plasma radiation in relation to the sample surface also influences the LIBS signal, mainly in two ways: (i) through the intensity of the overall collected light, as well as through the relative intensities of the emission lines and (ii) by observation of emission lines in one position,

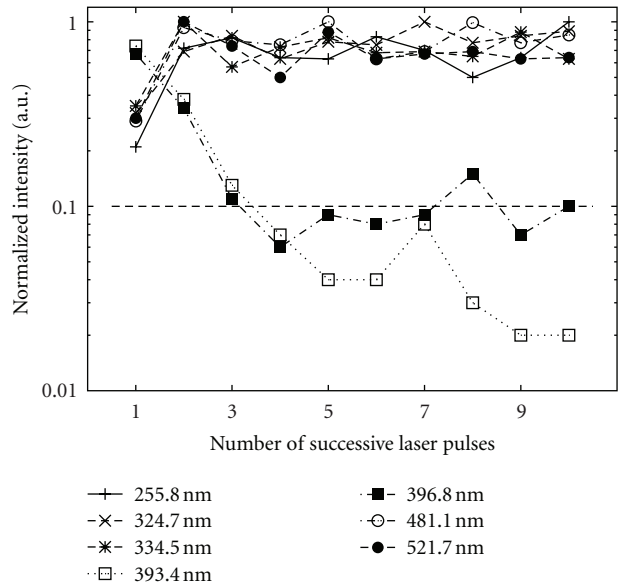

Figure 4: The relationship between the number of pulses in the same spot and the intensity of selected lines obtained by ablation of a brass sample at 0.32 μs. Intensities are from neutral copper (324.7 nm and 521.7 nm), neutral zinc (334.5 nm and 481.1 nm), and singly ionized zinc (255.8 nm). Emission lines at 393.4 and 396.8 nm belong to an unidentified pollutant on the surface of the target. The horizontal dashed line is the background level.

but not in the other, due to plasma heterogeneity. Present experiments were conducted in space integrating mode, in order to study the possibility of elemental detection by LIBS regardless of the collecting optics placement. Optical fiber collected the plasma light from its entire volume, but the position of the fiber (0.5 mm above the sample surface or 10 mm above it) showed some differences in the signal. The most noticeable difference was the different intensity levels of the strong copper and zinc emission lines. To overcome this and obtain spectra comparable in intensity with the fiber in both positions, the detector was operated at 100 times gain for the position 0.5 mm above the target surface and 200 times gain for the case when it was placed 10 mm away. This resulted in the detection of a larger number of emission lines for the latter case, as shown in Figure 5, which depicts an overlay of a portion of three spectra for each fiber position. The copper lines at 515.3 nm and 521.8 nm are consistent in both cases, although the intensity variation is larger for the case when the fiber is further from the surface of the target. The numerous peaks that are present for the fiber placed at 10 mm are random, but their high intensities compromise the automatic detection of elements. For example, emissions at 514.3 nm, 514.8 nm, and 516.5 nm have comparable intensities with the copper line at 515.3 nm, but they are observed only in one spectrum. It is estimated that for the spectra collected at this particular time (1.28 μs after plasma generation), the averaging of at least five spectra is needed in order to determine their effect as negligible, as compared for three spectra obtained from the fiber placed just above the target surface. On the other hand, the ratio of the intensities and of

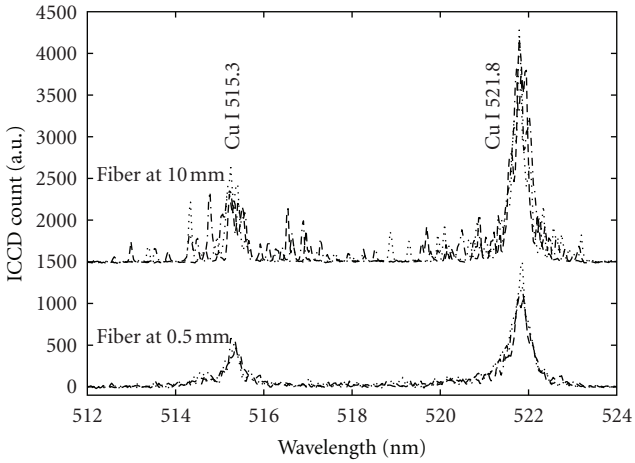

Figure 5: Three single-shot spectra for each fiber position obtained at 1.28 μs after laser ablation of brass (shifted for clarity, with the intensity preserved).

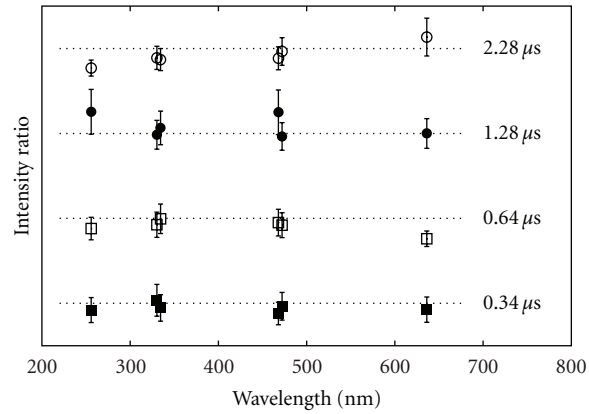

Figure 6: Intensity ratio $I_{@0.5}/I_{@10}$ of zinc lines between spectra obtained from two different fiber positions (horizontal lines equal 1, but are shifted for clarity). Data points correspond to lines Zn II 255.8 nm, Zn I 330.3 nm, Zn I 334.5 nm, Zn I 468.0 nm, Zn I 472.2 nm, and Zn I 636.2 nm.

the strong copper and zinc lines showed no difference regardless of the position of the fiber, as shown in Figure 6. Here, each data point is the ratio of the normalized intensities of zinc emission lines for a given wavelength from spectra collected at two different fiber positions; that is, the spectra of brass samples were normalized with regards to the intensity of the emission line at 481.0 nm, and then the value of the maximal intensity of a particular emission line obtained with the fiber close to the surface of the sample is divided by the value of the maximal intensity of the spectra at exactly the same wavelength obtained when the fiber is placed far from the sample. The points are shifted for clarity based on the time, and error bars correspond to 35% of the value of the point. This value is chosen to represent the error because it corresponds to the largest value for fractional error when the standard deviation of all points is considered. The same feature is obtained even for copper emission lines. The figure shows that although the fiber is placed in two different positions and sees the plasma at two different angles, the relative intensities of the emitted lines can be considered constant, since their ratios are fairly close to 1, confirming that the light-collecting setup was truly space integrated. The same feature is observed for line widths as well. Also, as before, copper lines emitted from copper sample and brass sample were completely the same in the range within the experimental error.

3.4. Temporal Evolution of Excited Atoms. Time evolution of the lines plays a crucial role in analyzing the spectra, because it reveals the behavior in time of the excited species and helps in identification of the plasma processes. As already stated, some strong lines, for example, lines at 330.3 nm and 330.7 nm, or line at 324.3 nm, although present at 0.34 μs after the creation of the plasma, are superimposed on the continuum but due to high free electron density are strongly broadened, showing large widths, and thus are not isolated. A general observation is that emissions from ionized atoms decreased in intensity more rapidly than the continuum radiation, while emissions from neutral atoms showed more complex histories, as is illustrated in Figure 7—emissions from ionized atoms—and Figure 8—emissions from neutral atoms. Out of several lines from ionized atoms, only the line at 255.8 nm could be observed even after 2.28 μs into the life of plasma, while the other zinc line at 250.2 nm disappears before 1.28 μs into the life of plasma. Lines of ionized copper are present at 1.28 μs but disappear before 2.28 μs, which is in agreement with the results presented by Német and Kozma [27]. There is a good agreement between our results and this reference even for emissions from neutral lines; this is illustrated, for example, by the rapid decrease of the intensity of the line at 327.4 nm and the slow increase of the intensity of line at 521.8 nm with time, both belonging to copper atoms. Also, the time when these two lines have equal intensities is before the first microsecond into the life of plasma. Both resonant and persistent copper emissions at 324.7 nm and 327.4 nm belong to the transition of the atom to the ground level and involve terms P-S (transition from the higher energy level $3d^{10}4p^1$ to the lower energy level $3d^{10}4s^1$), hence their rapid decrease in intensity. These lines are prone to self-absorption effects, and they reveal the high density of these atoms by the intensity ratio I (327.4 nm)/I (324.7 nm) which is about 1.8, instead of 1. Another transition that starts at the earliest moment in the life of copper plasma is the one that involves terms P-D, namely, the emission at 510.5 nm (from $3d^{10}4p^1$ to $3d^94s^2$). Indeed, this line is observed, but with a meager intensity. The only simultaneously persistent and resonant zinc line (transition from $4s^2$ to $4s^14p^1$, with emission at 307.6 nm) was not observed at all. The transitions that occur later in time, that is, those involving terms D-P and which appear at wavelengths 515.3 nm and 521.8 nm, for copper (transitions from $3d^{10}4d^1$ to $3d^{10}4p^1$), and at 334.5 nm and 636.2 nm for zinc (from $4s^14d^1$ to $4s^14p^1$), were clearly observed. The zinc line of the same type at 280.1 nm (from $4s^15d^1$ to $4s^14p^1$) was not observed at the initial moments, because it was buried under the continuum radiation, but it became distinct after 1.28 μs, albeit

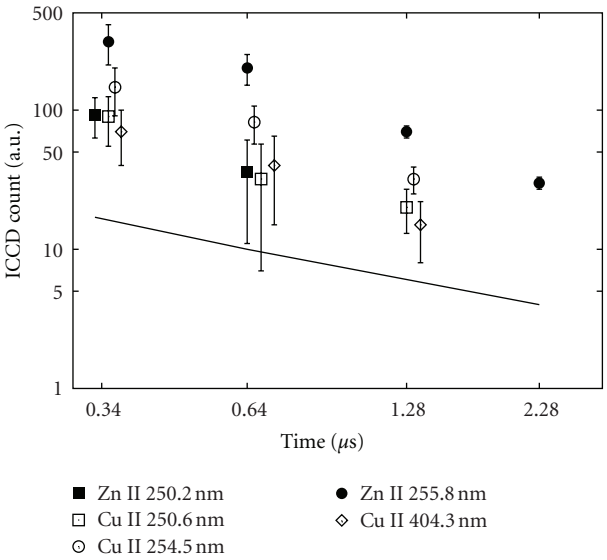

Figure 7: Temporal variation of line intensities for ionic emissions. Full symbols correspond to zinc emissions and open symbols correspond to copper emissions, while the line shows the background (continuum) level. Data points are slightly shifted in the time axis in order to be visible and not overlap.

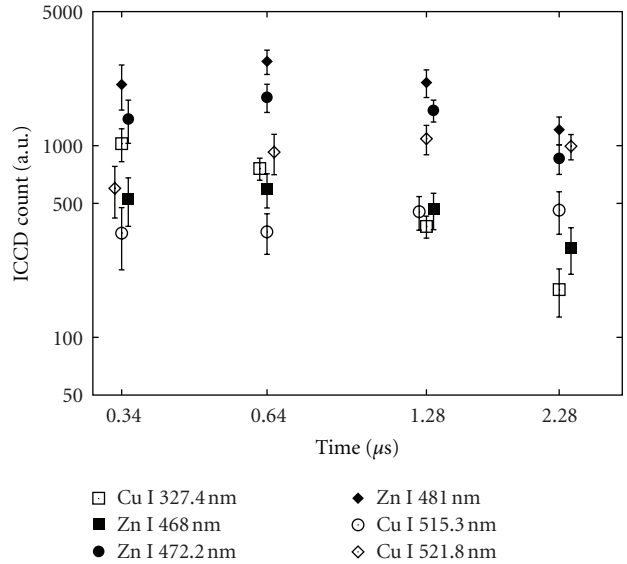

Figure 8: Temporal variation of line intensities for neutral emissions. Full symbols correspond to zinc emissions and open symbols correspond to copper emissions. Data points are slightly shifted in the time axis in order to be visible and not overlap.

with very wide line width. Zinc triple line emissions at 468.0 nm, 472.2 nm, and 481.0 nm which belong to the S-P transitions (from higher energy level $4s^1 5s^1$ to lower energy level $4s^1 4p^1$) were observed clearly during the entire time of investigation of plasma. These lines did not show large variation in intensity with time and, similarly to other zinc lines (330.2 nm and 334.5 nm), reached maximum values at 0.64 μs after the plasma generation. It should be noted that ionized zinc emissions are of the same transition terms S-P.

3.5. Plasma Temperature and Electron Density. Qualitative analysis of the plasma, that is, identification of elements, can be achieved without regard for the state of the plasma. Characterizing plasma by measuring its electron density and temperature, on the other hand, is a much more demanding task and requires fulfillment of several conditions. In LIBS experiments, electron density and temperature are usually calculated by experimentally measuring the Stark broadening of line width and through the Boltzmann plot, which are explained in detail in numerous books and articles, notably in [25]. Two important conditions are that the plasma should be in a state of local thermodynamic equilibrium (LTE), in which case the emissions from electron collisions are much larger than from the radiative processes, and plasma should be optically thin for the lines that are used for its characterization, which means that all emitted photons should escape the plasma volume. In our experiments, the second condition is tested by measuring the intensity ratios of the triplet of zinc emitting at 468.0 nm, 472.2 nm, and 481.0 nm and copper lines at 515.3 nm, 521.8 nm, and 578.2 nm, with none of these lines being resonant. The ratios of these lines are consistent with the transition probability ratios of the upper energy levels, as shown in Table 1. The change of line width with regard to fiber position was not considered for testing the optical thickness of the plasma, because, although the line width was the same in both fiber positions (fiber at 0.5 mm and at 10 mm from the target), this only confirmed the spatially integrated signal. Also, copper emission lines from both samples, pure copper and brass, showed the same intensities and line widths (see, e.g., copper lines in Figure 2), thus inferring that the optical depth did not change with the change of the concentration of the emitting element, in this case copper.

Table 1: Transition probability ratios.

		This work	NIST database
Cu lines from copper sample	521.8/515.3	1.42 ± 0.21	1.25
Cu lines from brass sample	521.8/515.3	1.51 ± 0.31	1.25
Zn lines from brass sample	481.0/472.2	1.55 ± 0.13	1.60
Zn lines from brass sample	481.0/468.0	4.26 ± 0.42	4.00
Zn lines from brass sample	330.2/334.5	1.14 ± 0.02	2.00

A rough estimate of electron number density and plasma temperature is possible, if the LTE is assumed. This assumption may be justified for our experimental conditions, because the gate time over which the plasma light is collected is 100 ns; that is, it is short enough for considering the rate change of the plasma temperature as negligible. In addition, the plasma is considered homogeneous in temperature and composition, as is confirmed by spatially integrated light collection and by experimenting with different target materials (copper and brass) while looking at the emission lines from the same type of element (neutral and ionized copper emissions).

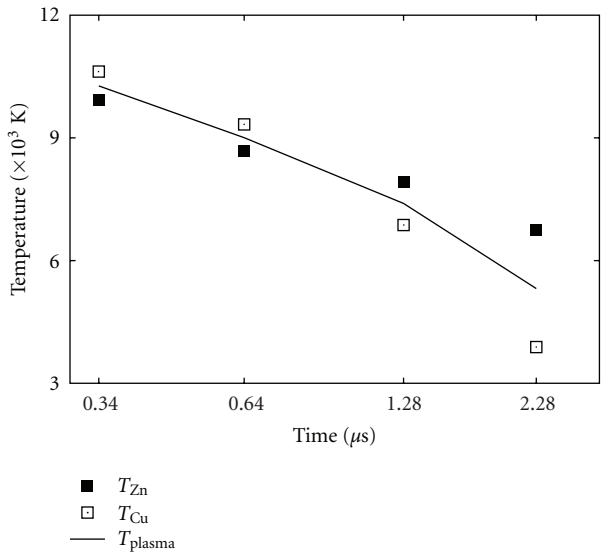

Figure 9: Temporal variation of the temperature obtained from the Bolztmann plot of the zinc (full symbols) and copper (open symbols). Full line is the average, thus denoting plasma excitation temperature.

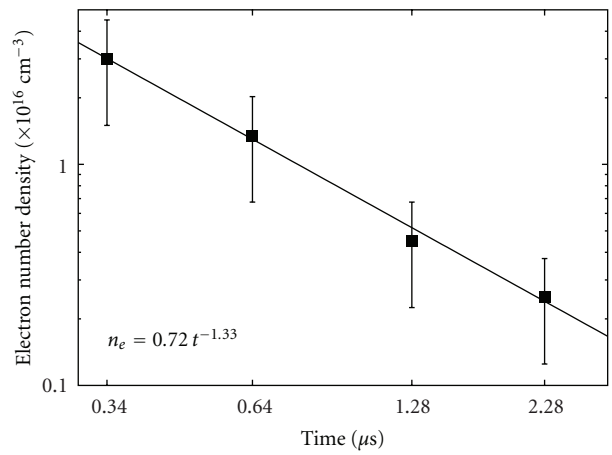

Figure 10: Temporal variation of electron number density obtained from the line width of the neutral zinc (472.2 nm).

The temperature of the plasma is calculated from the Boltzmann plot using integrated intensities of several non-resonant and well-resolved copper (578.2 nm, 515.3 nm, 521.8 nm, 458.7 nm, and 427.5 nm) and zinc lines (330.3 nm, 334.5 nm, 468.1 nm, 472.2 nm, and 481.0 nm), and the temperature evolution with time is shown in Figure 9. Plasma temperature is the average of the temperature calculated from zinc and copper emission lines. For calculation of electron number density, we fitted a Lorentzian curve to the zinc line at 472.2 nm and assumed that only the Stark effect causes line broadening. In this case, the line width at FWHM is given by

$$\Delta\lambda_{\text{Stark}} = 2\omega \frac{n_e}{10^{16}}, \tag{1}$$

where ω is the electron impact width parameter and n_e is the electron number density. In this work, $\omega = 0.1$ nm throughout the investigated time [28]. The change of the electron number density with time is shown in Figure 10. A power curve fit to the data shows that the electron number density decreases as $n_e \propto t^{-1.33}$. Comparison of the temperature and electron number density shows that the necessary condition for the application of local thermodynamic equilibrium (McWhirters criterion) is satisfied.

4. Conclusion

In this paper, time-resolved and spatially integrated LIBS experiments in brass and copper samples are presented. Different signals from both samples showed that the system can be used in discriminating different elemental compositions of the samples, although this can be done only at certain optimal times, that is, after the continuum radiation from inverse bremsstrahlung and free-free electron transitions have ceased and the free-bound or bound-bound electron transitions become dominant mechanisms for radiation. Based on several line emissions from both main constituents of brass alloy copper and zinc, we obtained comparable plasma temperature, while electron number density was estimated based on the zinc emission line at 472.2 nm. The merit of subsequent irradiation of the same spot was shown to be the removal of impurities, as well as a slight increase in the signal intensities. Different positions of the collecting optical fiber showed that there is no difference for elemental analysis, which means that all elements from the samples were observed in both tested fiber positions, thus confirming the applicability of the LIBS system without the need for sample position preparation. However, plasma showed different characteristics based on the fiber position; the most noticeable aspect was the decrease of the line intensity further away from the target surface. With regard to copper emission lines, comparison of spectra obtained from copper and brass samples showed no difference.

Acknowledgments

This work was carried out while the author was with Seoul National University and was supported by the Korean National Research Foundation—National Space Laboratory Grant (2009) contracted through IAAT and ERI at Seoul National University and Brain Korea 21 program.

References

[1] D. A. Cremers and L. J. Radziemski, *Handbook of Laser-Induced Breakdown Spectroscopy*, John Wiley & Sons, Chichester, UK, 2006.

[2] A. W. Miziolek, V. Palleschi, and I. Schechter, Eds., *Laser-Induced Breakdown Spectroscopy*, Cambridge University Press, Cambridge, UK, 2006.

[3] J. P. Singh and S. N. Thakur, Eds., *Laser-Induced Breakdown Spectroscopy*, Elsevier Science, Amsterdam, The Netherlands, 2007.

[4] C. Pasquini, J. Cortez, L. M. C. Silva, and F. B. Gonzaga, "Laser induced breakdown spectroscopy," *Journal of the Brazilian Chemical Society*, vol. 18, no. 3, pp. 463–512, 2007.

[5] C. Aragón and J. A. Aguilera, "Characterization of laser induced plasmas by optical emission spectroscopy: a review of experiments and methods," *Spectrochimica Acta B*, vol. 63, no. 9, pp. 893–916, 2008.

[6] D. W. Hahn and N. Omenetto, "Laser-induced breakdown spectroscopy (LIBS), part I: review of basic diagnostics and plasmaparticle interactions: still-challenging issues within the analytical plasma community," *Applied Spectroscopy*, vol. 64, no. 12, pp. 335A–366A, 2010.

[7] I. Rauschenbach, E. K. Jessberger, S. G. Pavlov, and H. W. Hübers, "Miniaturized laser-induced breakdown spectroscopy for the in-situ analysis of the martian surface: calibration and quantification," *Spectrochimica Acta B*, vol. 65, no. 8, pp. 758–768, 2010.

[8] N. L. Lanza, R. C. Wiens, S. M. Clegg et al., "Calibrating the ChemCam laser-induced breakdown spectroscopy instrument for carbonate minerals on Mars," *Applied Optics*, vol. 49, no. 13, pp. C211–C217, 2010.

[9] R. E. Russo, X. L. Mao, C. Liu, and J. Gonzalez, "Laser assisted plasma spectrochemistry: laser ablation," *Journal of Analytical Atomic Spectrometry*, vol. 19, no. 9, pp. 1084–1089, 2004.

[10] L. Fornarini, V. Spizzichino, F. Colao, R. Fantoni, and V. Lazic, "Influence of laser wavelength on LIBS diagnostics applied to the analysis of ancient bronzes," *Analytical and Bioanalytical Chemistry*, vol. 385, no. 2, pp. 272–280, 2006.

[11] N. M. Shaikh, S. Hafeez, and M. A. Baig, "Comparison of zinc and cadmium plasma parameters produced by laser-ablation," *Spectrochimica Acta B*, vol. 62, no. 12, pp. 1311–1320, 2007.

[12] R. Qindeel, M. S. Dimitrijevic, N. M. Shaikh, N. Bidin, and Y. M. Daud, "Spectroscopic estimation of electron temperature and density of zinc plasma open air induced by Nd: YAG laser," *The European Physical Journal Applied Physics*, vol. 50, no. 3, Article ID 30701, pp. 1–7, 2010.

[13] G. Cristoforetti, S. Legnaioli, V. Palleschi, A. Salvetti, and E. Tognoni, "Influence of ambient gas pressure on laser-induced breakdown spectroscopy technique in the parallel double-pulse configuration," *Spectrochimica Acta B*, vol. 59, no. 12, pp. 1907–1917, 2004.

[14] G. W. Rieger, M. Taschuk, Y. Y. Tsui, and R. Fedosejevs, "Comparative study of laser-induced plasma emission from micro-joule picosecond and nanosecond KrF-laser pulses," *Spectrochimica Acta B*, vol. 58, no. 3, pp. 497–510, 2003.

[15] B. Le Drogoff, M. Chaker, J. Margot et al., "Influence of the laser pulse duration on spectrochemical analysis of solids by laser-induced plasma spectroscopy," *Applied Spectroscopy*, vol. 58, no. 1, pp. 122–129, 2004.

[16] V. K. Unnikrishnan, K. Alti, R. Nayak et al., "Optimized LIBS setup with echelle spectrograph-ICCD system for multi-elemental analysis," *Journal of Instrumentation*, vol. 5, no. 4, Article ID P04005, pp. 1–16, 2010.

[17] X. L. Mao, A. C. Ciocan, and R. E. Russo, "Preferential vaporization during laser ablation inductively coupled plasma atomic emission spectroscopy," *Applied Spectroscopy*, vol. 52, no. 7, pp. 913–918, 1998.

[18] M. Gagean and J. M. Mermet, "Study of laser ablation of brass materials using inductively coupled plasma atomic emission spectrometric detection," *Spectrochimica Acta B*, vol. 53, no. 4, pp. 581–591, 1998.

[19] O. V. Borisov, X. L. Mao, A. Fernandez, M. Caetano, and R. E. Russo, "Inductively coupled plasma mass spectrometric study of non-linear calibration behavior during laser ablation of binary Cu–Zn alloys," *Spectrochimica Acta B*, vol. 54, no. 9, pp. 1351–1365, 1999.

[20] V. Margetic, A. Pakulev, A. Stockhaus, M. Bolshov, K. Niemax, and R. Hergenröder, "Comparison of nanosecond and femtosecond laser-induced plasma spectroscopy of brass samples," *Spectrochimica Acta B*, vol. 55, no. 11, pp. 1771–1785, 2000.

[21] V. Margetic, K. Niemax, and R. Hergenröder, "A study of non-linear calibration graphs for brass with femtosecond laser-induced breakdown spectroscopy," *Spectrochimica Acta B*, vol. 56, no. 6, pp. 1003–1010, 2001.

[22] C. Liu, X. L. Mao, S. S. Mao, X. Zeng, R. Greif, and R. E. Russo, "Nanosecond and femtosecond laser ablation of brass: particulate and ICPMS measurements," *Analytical Chemistry*, vol. 76, no. 2, pp. 379–383, 2004.

[23] A. B. Gojani and J. J. Yoh, "New ablation experiment aimed at metal expulsion at the hydrodynamic regime," *Applied Surface Science*, vol. 255, no. 22, pp. 9268–9272, 2009.

[24] Y. Ralchenko, A. E. Kramida, J. Reader, and NIST ASD Team, "NIST Atomic Spectra Database (version 4.0)," http://physics.nist.gov/asd, 2012.

[25] A. Thorne, U. Litzen, and S. Johanson, *Spectrophysics: Principles and Applications*, Springer, Berlin, Germany, 2nd edition, 1999.

[26] L. J. Radziemski and D. A. Cremers, "Spectrochemical analysis using laser plasma excitation," in *Laser-Induced Plasmas and Applications*, L. J. Radziemski and D. A. Cremers, Eds., chapter 7, p. 298, Marcel Dekker, New York, NY, USA, 1989.

[27] B. Német and L. Kozma, "Time-resolved optical emission spectrometry of Q-switched Nd: YAG laser-induced plasmas from copper targets in air at atmospheric pressure," *Spectrochimica Acta B*, vol. 50, no. 14, pp. 1869–1888, 1995.

[28] M. S. Dimitrijević and S. Sahal-Bréchot, "Stark broadening of neutral zinc spectral lines," *Astronomy and Astrophysics Supplement Series*, vol. 140, no. 2, pp. 193–196, 1999.